TITLE

Crystal structure of human endothelin ET_B receptor in complex with peptide inverse agonist IRL2500.

Chisae Nagiri[1*], Wataru Shihoya[1*‡], Asuka Inoue[2], Francois Marie Ngako Kadji[2], Junken Aoki[2], Osamu Nureki[1‡].

Affiliations:

[1] *Department of Biological Sciences, Graduate School of Science, The University of Tokyo, Bunkyo, Tokyo 113-0033, Japan.*

[2] *Graduate School of Pharmaceutical Sciences, Tohoku University, 6-3, Aoba, Aramaki, Aoba-ku, Sendai, Miyagi 980-8578, Japan.*

*These authors contributed equally to this work.

‡To whom correspondence should be addressed. E-mail: wtrshh9@gmail.com (W.S.), nureki@bs.s.u-tokyo.ac.jp (O.N.)

Abstract

Endothelin receptors (ET_A and ET_B) are G-protein coupled receptors activated by endothelin-1 and are involved in blood pressure regulation. IRL2500 is a peptide-mimetic of the C-terminal tripeptide of endothelin-1, and has been characterized as a potent ET_B-selective antagonist, which has preventive effects against brain edema. Here, we report the crystal structure of the human ET_B receptor in complex with IRL2500 at 2.7 Å-resolution. The structure revealed the different binding modes between IRL2500 and ET-1, and provides structural insights into its ET_B-selectivity. Notably, the biphenyl group of IRL2500 penetrates into the transmembrane core proximal to D2.50, stabilizing the inactive conformation. Using the newly-established constitutively active mutant, we clearly demonstrate that IRL2500 functions as an inverse agonist for the ET_B receptor. The current findings will expand the chemical space of ETR antagonists and facilitate the design of inverse agonists for other class A GPCRs.

Main text

Introduction

Endothelin receptors (ETR) are G-protein coupled receptors activated by vaso active peptide, endothelins[1]. Two endothelin receptor subtypes (ET_A and ET_B) are widely expressed in the vascular endothelium, brain, and other circulatory organs[2,3]. Endothelin-1 (ET-1) activates the endothelin receptors (ETRs) with sub-nanomolar affinities. The activation of the ET_A receptor leads to potent and long-lasting vasoconstriction, whereas that of the ET_B receptor induces nitric oxide-mediated vasorelaxation. Therefore, the up-regulation of ET-1 is significantly related to circulatory-system diseases, including pulmonary arterial hypertension (PAH)[4–7]. Moreover, the autocrine and paracrine signaling functions of ET-1 through the ET_A receptor play a critical role in tumor growth and survival[8]. Therefore, ETR antagonists have been developed for the treatment of circulatory-system diseases and cancers[6,7]. Bosentan is the first orally-active ETR antagonist[9,10], and is used to treat PAH. The ET_B receptor is the prominent ET receptor subtype in the brain, with high expression levels in astrocytes[11]. Stimulation of the ET_B receptor modulates astrocytic responses, indicating its important roles in regulating astrocytic functions[12]. The up-regulation of the astrocytic ET_B receptor by ET-1 increases the vascular permeability and reduces the AQP4 levels, thereby aggravating vasogenic brain edema[11]. The application of ET_B-selective antagonists may provide preventive effects against brain edema in the acute phase of brain insults[13–16].

To date, most endothelin receptor antagonists have been developed based on bosentan[17,18]. The ETR antagonists that have been developed till now are mostly N-

heterocyclic sulfonamides with similar structures and molecular weights, and non-sulfonamide antagonists (atrasentan, ambrisentan, darusentan, and enrasentan) still retain high similarities with each other and with the sulfonamides[7]. Therefore, the ETR agents are chemically very similar, and expanded chemical space should be exploited. IRL2500 is a peptide ETR antagonist developed based on the partial structure of ET-1[19], rather than bosentan. IRL2500 has been characterized as an ET_B-selective antagonist with an IC_{50} value of 1.2 nM[20], which shows higher affinity than that of bosentan. In an animal model, the intracerebroventricular administration of IRL2500 attenuated cold injury-mediated brain edema and disruption of the blood-brain barrier, indicating the neuroprotective effect of IRL2500[14,15]. An understanding of the IRL2500 binding mode would facilitate the expansion of the chemical space of ET agents.

We previously reported the crystal structures of the ET_B receptor bound to ET-1[21] and bosentan[22]; however, both the binding mode and ET_B-selectivity of IRL2500 remained to be elucidated. Here, we present the crystal structure of the ET_B receptor in complex with IRL2500. This structure revealed the unique binding mode of IRL2500, which differs from those of ET-1 and bosentan. Structure-guided functional analyses clearly demonstrate that IRL2500 functions as an inverse agonist for the ET_B receptor, and thus will provide the basis for design of inverse agonists for other class A GPCRs.

Results

Overall structure

For crystallization, we used the previously established, thermostabilized ET_B receptor (ET_B-Y4)[22,23]. The IC_{50} value of IRL2500 for ET_B-Y4 was similar to that for the wild type receptor in the TGFα shedding assay[24] (Fig. 1), suggesting that the themostabilizing mutations minimally affect the IRL2500 binding. In contrast, the IC_{50} value of IRL2500 for the ET_A receptor is over 3 μM (Fig. 1), indicating that IRL2500 has over 100-fold ET_B-selectivity, consistent with the previous pharmacological analysis[20]. To facilitate crystallization, we replaced the third intracellular loop (ICL3) of the receptor with minimal T4 Lysozyme[25] (ET_B-Y4-mT4L). Using *in meso* crystallization[26], we obtained crystals of ET_B-Y4-mT4L in complex with IRL2500 (Supplementary Fig. 1a, b). In total, 58 datasets were collected and merged by the data processing system KAMO[27]. Eventually, we determined the ET_B structure in complex with IRL2500 at 2.7 Å resolution, by molecular replacement using the antagonist-bound ET_B structure (PDB code: 5X93) (Table 1).

The overall structure consists of the canonical 7 transmembrane helices (TM), the amphipathic helix 8 at the C-terminus (H8), and two antiparallel β-strands in the extracellular loop 2 (ECL2), as in the previously determined ET_B structures (Fig. 2a). The IRL2500-bound structure is similar to the bosentan-bound structure, rather than the ET-1-bound structure (R.M.S.D. values for Cα atoms=1.34 and 1.95 Å, respectively), reflecting the inactive conformation. We observed a remarkable difference in the conformation of ECL2. The β strands are opened up by 9 Å, as compared with those in

the ligand-free structure (Fig. 2b and Supplementary Fig. 2a), and are the widest among the peptide-activated class A GPCRs (Supplementary Fig. 2b). This structural feature indicates the innate flexibility of ECL2, to capture the large peptide ligand endothelin, in the inactive conformation of the ET_B receptor.

IRL2500 binding site

We first describe the IRL2500 binding mode. IRL2500 consists of a tryptophan, a 3,5-dimethylbenzoyl group, and a biphenyl group[19], which are connected by two peptide bonds (Fig. 2c). IRL2500 binds to the transmembrane binding cleft exposed to the extracellular side, with a clear electron density in the $F_o - F_c$ omit map (Supplementary Fig. 3a, b). The carboxylate group of the tryptophan moiety in IRL2500 forms salt bridges with K182$^{3.33}$ and R343$^{6.55}$ (superscripts indicate Ballesteros–Weinstein numbers[28]) (Fig. 2c, d). The tryptophan side chain of IRL2500 hydrogen bonds with the carbonyl group of the N158$^{2.61}$ side chain, and forms extensive van der Waals interactions with N158$^{2.61}$, K161$^{2.64}$, V177$^{3.28}$, P178$^{3.29}$, and F240$^{4.64}$ (Fig. 2d). The dimethyl phenyl group of IRL2500 forms van der Waals interactions with the hydrophobic pocket, and is surrounded by V185$^{3.36}$, L277$^{5.42}$, Y281$^{5.46}$, W336$^{6.48}$, L339$^{6.51}$, and H340$^{6.52}$. The biphenyl group penetrates deeply into the receptor core proximal to D147$^{2.50}$, and forms van der Waals interactions with D147$^{2.50}$, H150$^{2.53}$, W336$^{6.48}$, and S376$^{7.43}$. Overall, the carboxylate of IRL2500 is specifically recognized by the positively charged residues of the ET_B receptor, and the other moieties fill the space within the transmembrane binding pocket.

To elucidate the structural basis for the ET_B-selectivity of IRL2500, we compared

the residues constituting the IRL2500 binding site between the ET_B and ET_A receptors (Fig. 3a and Supplementary Fig. 4). Although most of the residues are conserved, three residues are replaced with bulkier residues in the ET_A receptor (H150Y, V177F, and S376T). These replacements may cause steric clashes with the aromatic groups of IRL2500 and reduce its affinity. To investigate this hypothesis, we measured the IC_{50} values of IRL2500 for the H150Y, V177F, and S346T ET_B receptor mutants. These mutants showed similar responses for ET-1 in the TGFα shedding assay (Supplementary Fig. 5), and only V177F showed a 4-fold higher IC_{50} value with IRL2500 (Fig. 3b). These data suggest that the V177F mutation in the ET_A receptor sterically clashes with the tryptophan moiety of IRL2500 and reduces its affinity, thus partially accounting for the ET_B-selectivity of IRL2500. This is consistent with the previous study, in which the replacement of the tryptophan moiety with the smaller valine residue in IRL2500 weakened its ET_B-selectivity[29].

Comparison of the binding modes of IRL2500, ET-1, and bosentan

IRL2500 is designed to mimic the Y13, F14, I19, I20, and W21 residues in ET-1, which play critical roles in ligand binding to the ET_B receptor[19]. The tryptophan and dimethyl phenyl group of IRL2500 seem to be equivalent to W21 and I20 in ET-1, respectively, while the biphenyl group of IRL2500 seems to be equivalent to F14 and I19 of ET-1. However, a comparison between IRL2500 and ET-1 binding revealed an unexpected difference in their binding interactions (Fig. 4a). The carboxylate of the tryptophan in IRL2500 superimposes well with that of W21 in ET-1, and is coordinated by similar positively charged residues. The tryptophan moiety and dimethyl phenyl group

of IRL2500 superimpose well with I20 and W21 of ET-1, respectively. In contrast, the biphenyl group of IRL2500 penetrates into the receptor core, in an opposite manner to the F14 and I19 of ET-1. Overall, the electrostatic interactions between the carboxylates and the positively charged residues are conserved in IRL2500 and ET-1 binding, but the other moieties form totally distinct interactions with the receptor. The volume of the ligand binding pocket in the ligand-free structure is large, thereby allowing the aromatic moieties of IRL2500 to flip.

IRL2500 has distinct chemical moieties as compared with bosentan, because IRL2500 was not developed based on bosentan. To reveal the similarities and differences in their binding modes, we compared the binding modes of IRL2500 and bosentan in detail (Fig. 4b, c). The carboxylate of IRL2500 and the sulfonamide of bosentan are similarly coordinated by the positively charged residue R343$^{6.55}$, suggesting that this electrostatic interaction is a common feature of the antagonist binding to the ET_B receptor. In addition, like bosentan, the aromatic moieties of IRL2500 fit within the local hydrophobic pockets in the ET_B receptor. Overall, IRL2500 has moieties that form similar binding interactions to those of bosentan. However, bosentan lacks the moiety corresponding to the biphenyl group of IRL2500, which deeply penetrates into the receptor core. Thus, IRL2500 fits into the pocket more tightly as compared with bosentan, contributing to its higher affinity.

IRL2500 function an inverse agonist for ET_B

To obtain mechanistic insights into the receptor inactivation by IRL2500, we compared the ET_B structures bound to ET-1, bosentan, and IRL2500. Previous structural

studies showed that ET-1 binding induces the inward moment of the extracellular portion of TM6 including W336$^{6.48}$, leading to receptor activation on the intracellular side[21] (Fig. 5a). Bosentan binding sterically prevents the inward motion of W336$^{6.48}$ with its 2-methoxyphenoxy group, and thus functions as an antagonist[22] (Fig. 5b). The dimethylphenyl group of IRL2500 superimposes well with the 2-methoxyphenoxy group of bosentan and similarly prevents the inward motion. Moreover, the dimethyl phenyl and biphenyl groups of IRL2500 sandwich the W336$^{6.48}$ side chain, tightly preventing its inward rotation. These observations suggest that IRL2500 strongly prevents the transition to the active state, as compared with bosentan, thereby possibly working as an inverse agonist that reduces the basal activity.

To investigate the inverse agonist activity of IRL2500 for the ET_B receptor, we first measured ligand-induced AP-TGFα release responses. The EC_{50} value of the agonist ET-1 was 0.11 nM, while IRL2500 and the antagonist bosentan did not change the receptor activation level (Fig. 5c). These data suggested that IRL2500 does not have the inverse agonist activity or that the assay is not sensitive enough to detect inverse agonist activity. Indeed, we observed that the basal activity of the ET_B receptor was very low in the assay (Fig. 5d) and thus we could not distinguish whether IRL2500 functions as an antagonist or an inverse agonist by this assay.

Therefore, we tried the same assay using a constitutively active mutant of the ET_B receptor. Constitutively active mutant GPCRs have been employed in pharmacological characterizations of inverse agonists[30], because such mutant GPCRs allow the assay to measure signals in a larger detection window. The substitution of the highly conserved L3.43 to glutamine has been identified as a causative activating mutation in the TSHR[31]

and CYSLTR2[32] genes, which are related to hyperthyroidism and uveal melanoma, respectively. Therefore, we transferred the L3.43Q mutation into ET_B (ET_B-L192$^{3.43}$Q) and examined its constitutive activity. We found that ET_B-L3.43Q induced spontaneous AP-TGFα release in a plasmid volume-dependent manner (Fig. 5d), indicating that L3.43Q works as a constitutive active mutation in the ET_B receptor. We evaluated the dose response effects of bosentan and IRL2500, using the constitutive active mutant ET_B-L3.43Q (Fig. 5e). Again, the antagonist bosentan did not change the receptor activation from the baseline level, whereas IRL2500 reduced the basal activity (EC_{50}=1.2 nM). These data indicate that IRL2500 works as a potent inverse agonist for the ET_B receptor, consistent with the structural observations. The biphenyl group of IRL2500 prevents the inward motion of W336$^{6.48}$ and stabilizes the inactive conformation, and thus IRL2500 functions as an inverse agonist.

206 ## Discussion

207 We have determined the crystal structure of the ET_B receptor in complex with the
208 peptide compound IRL2500, and thus elucidated the detailed receptor interactions and
209 the structural basis for its ET_B selectivity. Although IRL2500 is designed to mimic the
210 partial structure of ET-1, the binding mode is quite different. Moreover, using the
211 constitutively active mutant that we established in the current study, we first revealed that
212 IRL2500 functions as a potent inverse agonist for the ET_B receptor, and provided the
213 structural basis for the inverse agonistic mechanism.

214 Small-molecule ETR antagonists have been developed over the years; however,
215 most ETR antagonists have been designed based on bosentan. Thus, the presently
216 available ET agents are chemically very similar. IRL2500 was developed based on ET-1
217 and has totally distinct chemical moieties, as compared with bosentan. However, the
218 comparison of the IRL2500 and bosentan binding modes revealed the unexpected
219 similarity in their binding interactions. This observation suggests that the charge-
220 complementary interactions in the center of the pocket form the core of the receptor-
221 antagonist interactions, and the other aromatic moieties fit the local hydrophobic pocket.
222 The ligand binding pocket in the inactive ET_B structures is larger than those in other
223 GPCR structures, and thus aromatic moieties may be necessary to fit well within the
224 pocket.

225 We revealed that the biphenyl group of IRL2500 penetrates deeply into the
226 receptor core proximal to $D147^{2.50}$, preventing the inward motion of $W336^{6.48}$ in TM6,
227 and thus IRL2500 functions as an inverse agonist (Fig. 6a). This D2.50 constitutes a

sodium binding site adjacent to the orthosteric site, which is highly conserved among the class A GPCRs[33]. Sodium has negative allosteric effects on ligand binding in most class A GPCRs, by stabilizing the inactive conformations. Therefore, this sodium binding site is the hot spot for the design of allosteric modulators and inverse agonists to fix receptors in the inactive conformations. In the BLT1 structure bound to the inverse agonist BIIL260, the benzamidine group of BIIL260 directly hydrogen bonds with D2.50, stabilizing the inactive conformation instead of the sodium[34] (Fig. 6b). The biphenyl group of IRL2500 superimposes well with the benzamidine group of BIIL260 (Fig. 6c). Although the biphenyl group of IRL2500 does not form any hydrogen-bonding interactions with the receptor, it prevents the conformational change around the D2.50 in a similar manner to the benzamidine moiety of BIIL260. For the design of effective inverse agonists, the biphenyl moiety would be also useful as a modulation part along with another moiety that exerts specific and tight binding to the orthosteric site, as well as a benzamidine group.

Materials and methods

Expression and purification

The haemagglutinin signal peptide, followed by the Flag epitope tag (DYKDDDDK) and a nine-amino-acid linker, was added to the N-terminus of the receptor, and a tobacco etch virus (TEV) protease recognition sequence was introduced between G57 and L66, to remove the disordered N-terminus during the purification process. The C-terminus was truncated after S407, and three cysteine residues were mutated to alanine (C396A, C400A, and C405A) to avoid heterogeneous palmitoylation. To improve crystallogenesis, we introduced four thermostabilizing mutations () and inserted minimal T4 lysozyme[25] into intracellular loop 3, between L303$^{5.68}$ and L311$^{6.23}$ (ET_B-Y4-mT4L[22]).

The thermostabilized construct ET_B-Y4-mT4L was subcloned into a modified pFastBac vector, with the resulting construct encoding a TEV cleavage site followed by a GFP-His[10] tag at the C-terminus. The recombinant baculovirus was prepared using the Bac-to-Bac baculovirus expression system (Invitrogen). Sf9 insect cells were infected with the virus at a cell density of 4.0×10^6 cells per millilitre in Sf900 II medium, and grown for 48 h at 27 °C. The harvested cells were disrupted by sonication, in buffer containing 20 mM Tris-HCl, pH 7.5, and 20% glycerol. The crude membrane fraction was collected by ultracentrifugation at 180,000*g* for 1 h. The membrane fraction was solubilized in buffer, containing 20 mM Tris-HCl, pH 7.5, 200 mM NaCl, 1% DDM, 0.2% cholesterol hemisuccinate, 10 μM IRL2500, and 2 mg ml^{-1} iodoacetamide, for 1 h at 4 °C. The supernatant was separated from the insoluble material by

ultracentrifugation at 180,000*g* for 20 min, and incubated with TALON resin (Clontech) for 30 min. The resin was washed with ten column volumes of buffer, containing 20 mM Tris-HCl, pH 7.5, 500 mM NaCl, 0.1% LMNG, 0.01% CHS, 10 μM IRL2500, and 15 mM imidazole. The receptor was eluted in buffer, containing 20 mM Tris-HCl, pH 7.5, 500 mM NaCl, 0.01% LMNG, 0.001% CHS, 10 μM IRL2500, and 200 mM imidazole. The eluate was treated with TEV protease and dialysed against buffer (20 mM Tris-HCl, pH 7.5, 500 mM NaCl, and 10 μM IRL2500). The cleaved GFP–His_{10} tag and the TEV protease were removed with Co^{2+}-NTA resin. The receptor was concentrated and loaded onto a Superdex200 10/300 Increase size-exclusion column, equilibrated in buffer containing 20 mM Tris-HCl, pH 7.5, 150 mM NaCl, 0.01% LMNG, 0.001% CHS, and 10 μM IRL2500. Peak fractions were pooled, concentrated to 40 mg ml^{-1} using a centrifugal filter device (Millipore 50 kDa MW cutoff), and frozen until crystallization. During the concentration, IRL2500 was added to a final concentration of 100 μM.

Crystallization

The purified receptor was reconstituted into molten lipid (monoolein and cholesterol 10:1 by mass) at a weight ratio of 1:1.5 (protein:lipid). The protein-laden mesophase was dispensed into 96-well glass plates in 30 nl drops and overlaid with 800 nl precipitant solution by a Gryphon LCP robot (Art Robbins Instruments)[26]. Crystals of ET_B-Y4-mT4L bound to IRL2500 were grown at 20ºC in precipitant conditions containing 30% PEG300, 100 mM Bis-tris, pH 7.5, 150 mM sodium phosphate monobasic, and 10 mM TCEP hydrochloride. The crystals were harvested directly from

293 the LCP using micromounts (MiTeGen) or LithoLoops (Protein Wave) and frozen in
294 liquid nitrogen, without adding any extra cryoprotectant.
295
296 **Data collection and structure determination**

297 X-ray diffraction data were collected at the SPring-8 beamline BL32XU, with 10
298 × 15 μm^2 (width × height) micro-focused beams and an EIGER X 9M detector (Dectris).
299 Various wedge data sets (10°) per crystal were mainly collected with the ZOO system, an
300 automatic data-collection system developed at SPring-8 (K.Y., G.U., K.H., M.Y., and
301 K.H., submitted). The loop-harvested microcrystals were identified by raster scanning
302 and subsequently analyzed by SHIKA[35]. Each data set was indexed and integrated with
303 XDS[36], and the datasets were hierarchically clustered by using the correlation coefficients
304 of the intensities between datasets. After the rejection of outliers, 58 data sets were finally
305 merged with XSCALE[36]. The IRL2500-bound structure was determined by molecular
306 replacement with PHASER[37], using the K8794-bound ET_B structure (PDB code: 5X93).
307 Subsequently, the model was rebuilt and refined using COOT[38] and PHENIX[39],
308 respectively. The final model of IRL2500-bound ET_B-Y4-T4L contained residues 91-207,
309 214-303, and 311-403 of ET_B, 1-14 and 22-117 of mT4L, IRL2500, 6 monoolein
310 molecules, two phosphoric acids, and 41 water molecules. The model quality was
311 assessed by MolProbity[40]. Figures were prepared using CueMol
312 (http://www.cuemol.org/ja/)
313

TGFα shedding assay

The TGFα shedding assay, which measures the activation of Gq and G12 signaling[24], was performed as described previously[22]. Briefly, a plasmid encoding an ET_B construct with an internal FLAG epitope tag or an ET_A construct was transfected, together with a plasmid encoding alkaline phosphatase (AP)-tagged TGFα (AP-TGFα), into HEK293A cells by using a polyethylenimine (PEI) transfection reagent (1 μg ETR plasmid, 2.5 μg AP-TGFα plasmid, and 25 μl of 1 mg/ml PEI solution per 10-cm culture dish). After a one day culture, the transfected cells were harvested by trypsinization, washed, and resuspended in 30 ml of Hank's Balanced Salt Solution (HBSS) containing 5 mM HEPES (pH 7.4). The cell suspension was seeded in a 96 well plate (cell plate) at a volume of 80 μl per well and incubated for 30 min in a CO_2 incubator. For the measurement of antagonist activity, IRL2500 was diluted in 0.01% bovine serum albumin (BSA) and HEPES-containing HBSS (assay buffer) and added to the cell plate at a volume of 10 μl per well. After 5 min, ET-1, at a final concentration of 0.2 nM, was added to the cell plate at a volume of 10 μl per well. For the measurement of agonistic activity, after adding 10 μl of the assay buffer, serially diluted ET-1 was mixed with the cells at a volume of 10 μl per well. After a 1 h incubation in the CO_2 incubator, aliquots of the conditioned media (80 μl) were transferred to an empty 96-well plate (conditioned media (CM) plate). Similarly, for the measurement of inverse agonist activity, the cells were mixed with 10 μl of the assay buffer, followed by the addition of serially diluted IRL2500, and incubated for 4 h before the transfer of the conditioned media. The AP reaction solution (10 mM *p*-nitrophenylphosphate (*p*-NPP), 120 mM Tris–HCl (pH 9.5), 40 mM NaCl, and 10 mM

336 $MgCl_2$) was dispensed into the cell plates and the CM plates (80 µl per well). The
337 absorbance at 405 nm (Abs_{405}) of the plates was measured, using a microplate reader
338 (SpectraMax 340 PC384, Molecular Devices), before and after a 1 h incubation at room
339 temperature. AP-TGFα release was calculated as described previously[22]. The AP-TGFα
340 release signals were fitted to a four-parameter sigmoidal concentration-response curve,
341 using the Prism 7 software (GraphPad Prism), and the pEC_{50} (equal to $-Log_{10}$ EC_{50}) and
342 E_{max} values were obtained.

343 To measure the constitutive activity in a plasmid volume-dependent manner,
344 HEK293 cells were seeded in a 96-well plate at a concentration of 4×10^5 cells per ml in
345 Opti-MEM I Reduced Serum Media (Thermo Fisher Scientific), in a volume of 80 µl per
346 well. A transfection mixture was prepared by mixing the PEI transfection reagent (0.2 µl
347 per well) and plasmids (20 ng AP-TGFα plasmid, titrated ETR plasmid, and an empty
348 vector to balance the total plasmid volume) in Opti-MEM I Reduced Serum Media (20
349 µl). The mixture was added to the cells, which were then incubated for 24 h before the
350 transfer of the conditioned media. After adding the AP reaction solution, the absorbances
351 of the cells and the CM plates were measured at 20 min intervals. The AP-TGFα release
352 signals were calculated as described above, and the signal in the mock-transfected
353 conditions was set at the baseline.
354
355
356

Acknowledgements

The diffraction experiments were performed at SPring-8 BL32XU (proposal 2017A2527). We thank the beamline staff at BL32XU of SPring-8 (Sayo, Japan) for technical assistance during data collection. We also thank Kouki Kawakami, Takeaki Shibata and Ayumi Inoue (Tohoku University, Japan) for technical assistance in the characterization of the L3.43Q-mutant ET_B receptor. This work was supported by grants from the Platform for Drug Discovery, Informatics and Structural Life Science by the Ministry of Education, Culture, Sports, Science and Technology (MEXT), JSPS KAKENHI grants 16H06294 (O.N.), 17J30010 (W.S.), 30809421 (W.S.), 17K08264 (A.I.), and the Japan Agency for Medical Research and Development (AMED) grants: the PRIME JP17gm5910013 (A.I.) and the LEAP JP17gm0010004 (A.I. and J.A.), and the National Institute of Biomedical Innovation.

Author contributions

C.N. expressed, purified, and crystallized the IRL2500-bound ET_B receptor, collected data, and refined the structures. W.S. designed all of the experiments, initially crystallized the receptor, and refined the structure. A.I., F.M.N.K., and J.A. performed and oversaw the cell-based assays. The manuscript was prepared by C.N., W.S., A.I., and O.N. W.S. and O.N. supervised the research. Coordinates and structure factors have been deposited in the Protein Data Bank, under the accession number XXXX for the IRL2500-bound structure. The X-ray diffraction images are also available at SBGrid Data Bank (https://data.sbgrid.org/), under the ID YYYY.

379

380 Competing interests

381 The authors declare no competing interests

References

1. Yanagisawa, M. *et al.* A novel potent vasoconstrictor peptide produced by vascular endothelial cells. *Nature* **332,** 411–415 (1988).
2. Arai, H. *et al.* Cloning and expression of a cDNA encoding an endothelin receptor. *Nature* **348,** 730–732 (1990).
3. Sakurai, T. *et al.* Cloning of a cDNA encoding a non-isopeptide-selective subtype of the endothelin receptor. *Nature* **348,** 732–735 (1990).
4. Channick, R. N. *et al.* Effects of the dual endothelin-receptor antagonist bosentan in patients with pulmonary hypertension: a randomised placebo-controlled study. *Lancet* **358,** 1119–1123 (2001).
5. Rubin, L. J. *et al.* Bosentan therapy for pulmonary arterial hypertension. *N. Engl. J. Med.* **346,** 896–903 (2002).
6. Maguire, J. J. & Davenport, A. P. Endothelin@25 - new agonists, antagonists, inhibitors and emerging research frontiers: IUPHAR Review 12. *Br. J. Pharmacol.* **171,** 5555–5572 (2014).
7. Davenport, A. P. *et al.* Endothelin. *Pharmacol. Rev.* **68,** 357–418 (2016).
8. Rosanò, L., Spinella, F. & Bagnato, A. Endothelin 1 in cancer: biological implications and therapeutic opportunities. *Nat. Rev. Cancer* **13,** 637–651 (2013).
9. Clozel, M. *et al.* Pathophysiological role of endothelin revealed by the first orally active endothelin receptor antagonist. *Nature* **365,** 759–761 (1993).
10. Clozel, M. *et al.* Pharmacological characterization of bosentan, a new potent orally active nonpeptide endothelin receptor antagonist. *J. Pharmacol. Exp. Ther.* **270,** 228–235 (1994).
11. Koyama, Y. & Michinaga, S. Regulations of Astrocytic Functions by Endothelins: Roles in the Pathophysiological Responses of Damaged Brains. *J. Pharmacol. Sci.* **118,** 401–407 (2012).
12. Hammond, T. R. *et al.* Endothelin-B Receptor Activation in Astrocytes Regulates the Rate of Oligodendrocyte Regeneration during Remyelination. *Cell Rep.* **13,** 2090–2097 (2015).
13. Moldes, O. *et al.* Neuroprotection afforded by antagonists of endothelin-1 receptors in experimental stroke. *Neuropharmacology* **63,** 1279–1285 (2012).
14. Michinaga, S. *et al.* Amelioration of Cold Injury-Induced Cortical Brain Edema Formation by Selective Endothelin ETB Receptor Antagonists in Mice. *PLoS*

One **9,** e102009 (2014).

15. Michinaga, S. *et al.* Improvement of cold injury-induced mouse brain edema by endothelin ET_B antagonists is accompanied by decreases in matrixmetalloproteinase 9 and vascular endothelial growth factor-A. *Eur. J. Neurosci.* **42,** 2356–2370 (2015).
16. Michinaga, S. *et al.* Delayed Administration of BQ788, an ET_B Antagonist, after Experimental Traumatic Brain Injury Promotes Recovery of Blood–Brain Barrier Function and a Reduction of Cerebral Edema in Mice. *J. Neurotrauma* **35,** 1481–1494 (2018).
17. Palmer, M. J. Endothelin Receptor Antagonists: Status and Learning 20 Years On. *Prog. Med. Chem.* **47,** 203–237 (2009).
18. Mucke, H. A. M. Small-molecule endothelin receptor antagonists: a review of patenting activity across therapeutic areas. *IDrugs* **12,** 366–375 (2009).
19. Friih, T. *et al.* IRL 2500: A potent ET_B selective endothelin antagonist. *Bioorganic Med. Chem. Lett.* **6,** 2323–2328 (1996).
20. Balwierczak, J. L. *et al.* Characterization of a potent and selective endothelin-B receptor antagonist, IRL 2500. *J. Cardiovasc. Pharmacol.* **26 Suppl 3,** S393-6 (1995).
21. Shihoya, W. *et al.* Activation mechanism of endothelin ET_B receptor by endothelin-1. *Nature* **537,** 363–368 (2016).
22. Shihoya, W. *et al.* X-ray structures of endothelin ET_B receptor bound to clinical antagonist bosentan and its analog. *Nat. Struct. Mol. Biol.* 24, 758–764 (2017).
23. Okuta, A. *et al.*Thermostabilization of the Human Endothelin Type B Receptor. *J. Mol. Biol.* **428,** 2265–2274 (2016).
24. Inoue, A. *et al.* TGFα shedding assay: an accurate and versatile method for detecting GPCR activation. *Nat. Methods* **9,** 1021–1029 (2012).
25. Thorsen, T. S. *et al.* Modified T4 Lysozyme Fusion Proteins Facilitate G Protein-Coupled Receptor Crystallogenesis. *Structure* **22,** 1657–1664 (2014).
26. Caffrey, M. & Cherezov, V. Crystallizing membrane proteins using lipidic mesophases. *Nat. Protoc.* **4,** 706–731 (2009).
27. Yamashita, K., Hirata, K. & Yamamoto, M. KAMO: towards automated data processing for microcrystals. *Acta Crystallogr. Sect. D Struct. Biol.* **74,** 441–449 (2018).
28. Ballesteros, J. A. & Weinstein, H. Integrated methods for the construction of three-dimensional models and computational probing of structure-function

relations in G protein-coupled receptors. *Methods Neurosci.* **25,** 366–428 (1995).

29. Sakaki, J. *et al.* Discovery of IRL 3461: a novel and potent endothelin antagonist with balanced ET_A/ET_B affinity. *Bioorg. Med. Chem. Lett.* **8,** 2241–2246 (1998).

30. Soudijn, W., van Wijngaarden, I. & Ijzerman, A. P. Structure-activity relationships of inverse agonists for G-protein-coupled receptors. *Med. Res. Rev.* **25,** 398–426 (2005).

31. Trülzsch, B. *et al.* Detection of thyroid-stimulating hormone receptor and Gsalpha mutations: in 75 toxic thyroid nodules by denaturing gradient gel electrophoresis. *J. Mol. Med.* **78,** 684–691 (2001).

32. Moore, A. R. *et al.* Recurrent activating mutations of G-protein-coupled receptor CYSLTR2 in uveal melanoma. *Nat. Genet.* **48,** 675–680 (2016).

33. Katritch, V. *et al.* Allosteric sodium in class A GPCR signaling. *Trends Biochem. Sci.* **39,** 233–244 (2014).

34. Hori, T. *et al.* Na^+-mimicking ligands stabilize the inactive state of leukotriene B4 receptor BLT1. *Nat. Chem. Biol.* **14,** 262–269 (2018).

35. Ueno, G. *et al.* Remote access and automation of SPring-8 MX beamlines. in *AIP Conf. Proc.* **1741,** 050021 (2016).

36. Kabsch, W. *XDS*. *Acta Crystallogr. D Biol. Crystallogr.* **66,** 125–132 (2010).

37. McCoy, A. J. *et al.* Phaser crystallographic software. *J. Appl. Crystallogr.* **40,** 658–674 (2007).

38. Emsley, P., Lohkamp, B., Scott, W. G. & Cowtan, K. Features and development of Coot. *Acta Crystallogr. D Biol. Crystallogr.* **66,** 486–501 (2010).

39. Adams, P. D. *et al.* PHENIX: a comprehensive Python-based system for macromolecular structure solution. *Acta Crystallogr. D Biol. Crystallogr.* **66,** 213–221 (2010).

40. Chen, V. B. *et al.* MolProbity: all-atom structure validation for macromolecular crystallography. *Acta Crystallogr. D Biol. Crystallogr.* **66,** 12–21 (2010).

Figure Legends

Fig. 1. Inhibition of ET-1 binding by IRL2500.

Effect of IRL2500 on the ET-1 (0.2 nM)-induced release of AP-TGFα in HEK293 cells expressing the endothelin receptors. For each experiment, the AP-TGFα release response in the absence of IRL2500 is set at 100%. Data are displayed as means ± s.e.m. (standard error of the mean) from seven to nine independent experiments, with each performed in triplicate.

Fig. 2. ET_B structure in complex with IRL2500.

a, The overall structure of the IRL2500-bound ET_B receptor. The receptor is shown as a sky blue ribbon model. IRL2500 is shown as a deep sky blue stick with a transparent surface model. **b**, Superimposition of the IRL2500-bound and ligand-free ET_B structures (PDB code: 5GLI), colored sky blue and light green, respectively. **c**, Schematic representation of the interactions between ET_B and IRL2500 within 4.5 Å. The dashed lines show hydrogen bonds. **d,** Binding pocket for IRL2500, viewed from the extracellular side (over) and the membrane plane (lower). The receptor is shown in a sky blue ribbon representation. IRL2500 and receptor residues involved in ligand binding are shown as sticks, coloured deep sky blue and sky blue, respectively. The dashed lines show hydrogen bonds.

503 **Fig. 3. Conservation of the IRL2500 binding site.**

504 **a**, Sequence conservation of the IRL2500 binding site between ET_A and ET_B, mapped
505 onto the IRL2500-bound structure. Conserved and non-conserved residues are coloured
506 sky blue and gray, respectively. The receptor residues involved in IRL2500 binding are
507 shown as sticks. The dashed lines show hydrogen bonds. **b**, Effect of IRL2500 on the ET-
508 1 (0.2 nM)-induced release of AP-TGFα in HEK293 cells expressing the mutant ET_B
509 receptors. For each experiment, the AP-TGFα release response in the absence of IRL2500
510 is set at 100%. Data are displayed as means ± s.e.m. (standard error of the mean) from
511 four to six independent experiments, with each performed in triplicate.
512
513 **Fig. 4. Comparison of binding modes of IRL2500, ET-1, and bosentan.**

514 **a,** Superimposition of the IRL2500- and ET-1-bound ET_B receptors (PDB code: 5GLH).
515 The ET-1- and IRL2500-bound receptors are shown as pink and sky blue ribbons,
516 respectively. IRL2500 is shown as a stick model. ET-1 is shown as a magenta ribbon with
517 stick models of the peptide residues (Y13, F14, I19, I20, and W21). **b, c,** Binding pockets
518 for bosentan (**b**) and IRL2500 (**c**). The bosentan-bound receptor (PDB code: 5XPR) is
519 shown as a thin orange ribbon model. The residues involved in bosentan binding ($D154^{2.57}$,
520 $Q181^{3.32}$, $K182^{3.33}$, $K273^{5.38}$, $W336^{6.48}$, and $R343^{6.55}$) and $D147^{2.50}$ are shown as sticks.
521 Bosentan is shown as an orange stick model. IRL2500 and the IRL2500-bound receptor
522 are coloured as in panel (**a**). The residues involved in IRL2500 binding ($N158^{2.61}$,
523 $K182^{3.33}$, $R343^{6.55}$, $D147^{2.50}$, and $W336^{6.48}$) are shown as sticks.
524

525 **Fig. 5. Inverse agonistic activity of IRL2500.**

526 **a, b,** Structural changes upon ET-1 and IRL2500 binding, as compared with the bosentan-
527 bound structure, coloured as in Fig. 4. Black arrows indicate the inward movements of
528 TM6 and W336$^{6.48}$. **c,** Effects of IRL2500 and bosentan on the ET-1-induced AP-TGFα
529 release for the ET_B receptor. Data are displayed as means ± s.e.m. (standard error of the
530 mean) from three to four independent experiments. **d,** Constitutive activity of ETB.
531 HEK293 cells were transfected with titrated volume of a plasmid encoding the wild-type
532 ET_B (ET_B-WT) or the L3.43Q-mutant ET_B (ET_B-L3.43Q) and accumulated AP-TGFα
533 release during 24 h after transfection was measured. AP-TGFα release signal in 0 ng
534 receptor plasmid was set as a baseline. Data are displayed as means ± s.e.m. from three
535 independent experiments.. **e,** Effects of IRL2500 and bosentan on the ET-1-induced AP-
536 TGFα release for the constitutive active ET_B receptor (ET_B-L3.43Q). Data are displayed
537 as means ± s.e.m. from three to four independent experiments.
538
539 **Fig. 6. Structural comparison of ET_B and BLT1 in complex with inverse**
540 **agonists.**

541 **a, b,** The overall structures of the IRL2500-bound ET_B receptor (**a**) and the BIIL260-
542 bound BLT1 receptor (PDB code: 5X33) (**b**). The ET_B and BLT1 receptors are shown as
543 sky blue and light green ribbons, respectively. The inverse agonists IRL2500 and BIIL260
544 are shown as blue and dark green sticks, respectively. The lower panels show the binding
545 interactions around the sodium binding site. The residues involved in ligand binding are
546 represented with sticks. Hydrogen bonds are indicated by black dashed lines. In the

IRL2500-bound structure, the biphenyl group of IRL2500 forms van der Waals interactions with the receptor, and does not form any hydrogen-binding interactions. In the BIIL260 structure, BIIL260 forms hydrogen bonds with $D66^{2.50}$, $S106^{3.39}$, and $S276^{7.45}$. **c,** Superimposition of the ET_B and BLT1 structures in complex with the inverse agonists.

Supplementary Figure Legends

Supplementary Fig. 1. Crystallization.

a, Gel filtration chromatogram and SDS-PAGE of the purified IRL2500-bound ET_B receptor. **b**, Crystals of the IRL2500-bound ET_B receptor.

Supplementary Fig. 2. Comparison of the ECL2 structure with those of other peptide-activated GPCRs.

a, Superimposition of the ET_B structures determined to date. The IRL2500-bound and other structures are coloured sky blue and gray, respectively. **b**, Superimposition of the IRL2500-bound ET_B structure with other peptide-activated class A GPCRs.

Supplementary Fig. 3. Electron density.

a, $F_o - F_c$ omit maps for IRL2500, contoured at 3.0σ. **b**, $2F_o - F_c$ map around the IRL2500 binding site, contoured at 2.5σ.

Supplementary Fig. 4. Alignment of the human ET_A and ET_B receptors.

Alignment of the amino acid sequences of the human ET_B receptor (UniProt ID: P24530) and the human ET_A receptor (P25101). Secondary structure elements for α-helices and β-strands are indicated by cylinders and arrows, respectively. Conservation of the residues between ET_A and ET_B is indicated as follows: red panels for completely conserved; red

583 letters for partially conserved; and black letters for not conserved. The residues involved
584 in IRL2500 binding are indicated with squares.
585
586 **Supplementary Fig. 5. ET-1 responses of mutant receptors.**

587 Concentration response-curves of AP-TGFα release in the ET-1 treatment of HEK293
588 cells expressing the endothelin receptors. Symbols and error bars are means and s.e.m.
589 (standard error of the mean) of four or six independent experiments, each performed in
590 triplicate.

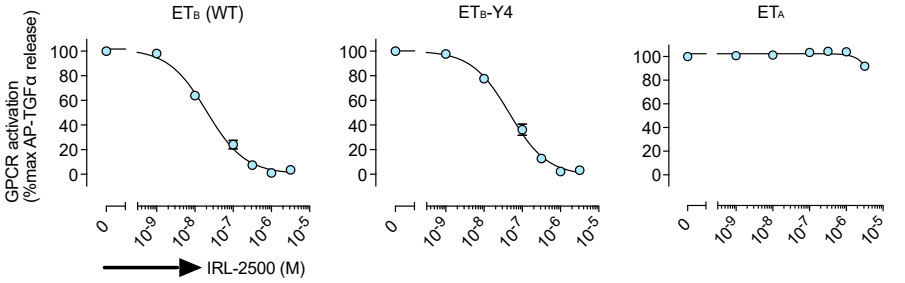

	ET_B (n=7)	ET_B-Y4 (n=8)	ET_A (n=9)
IC_{50} (pIC_{50} ± SEM)	20 nM (7.70 ± 0.05)	44 nM (7.35 ± 0.07)	> 3 µM (>5.5)

Nagiri et al. Figure 1

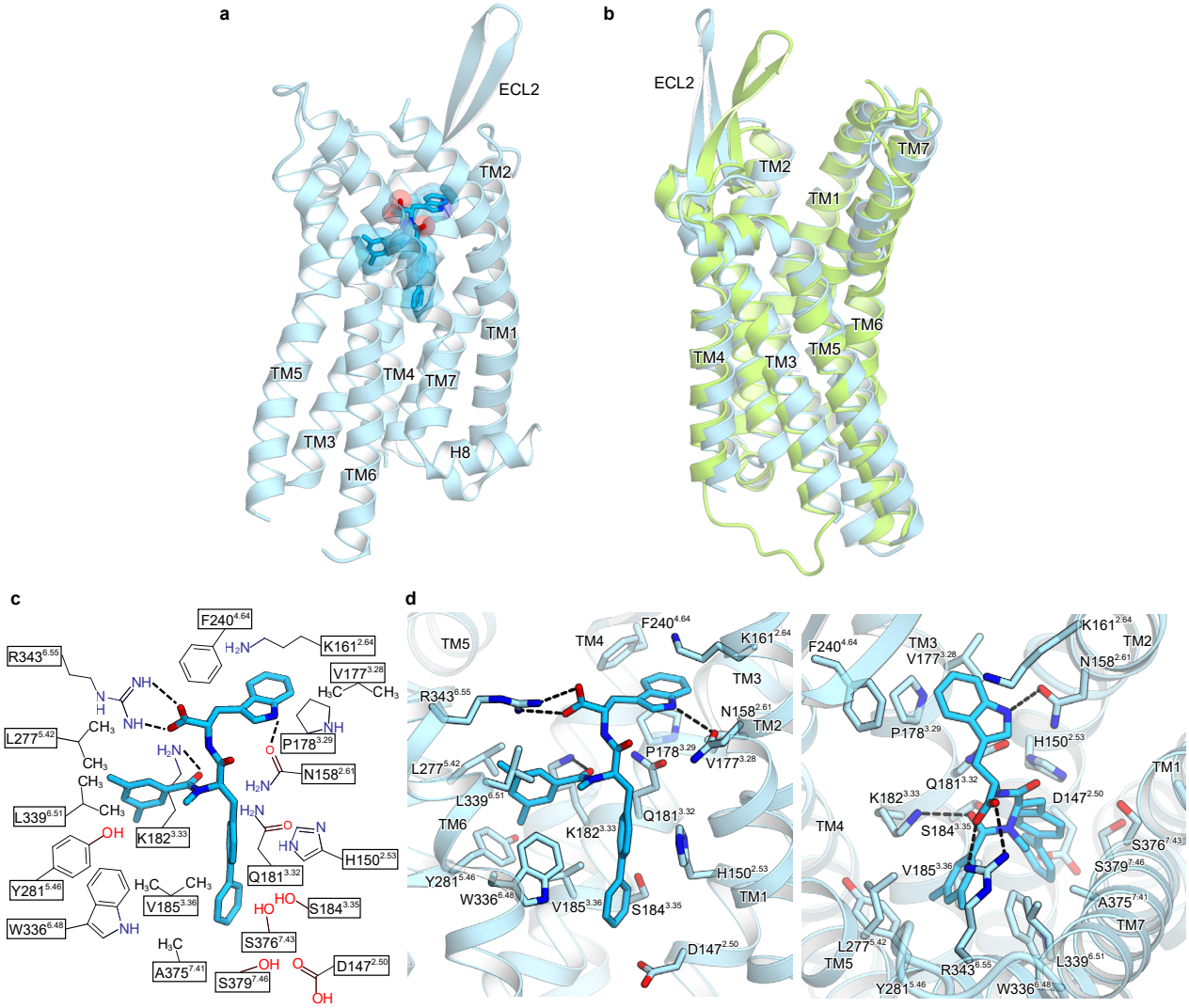

Nagiri et al. Figure 2

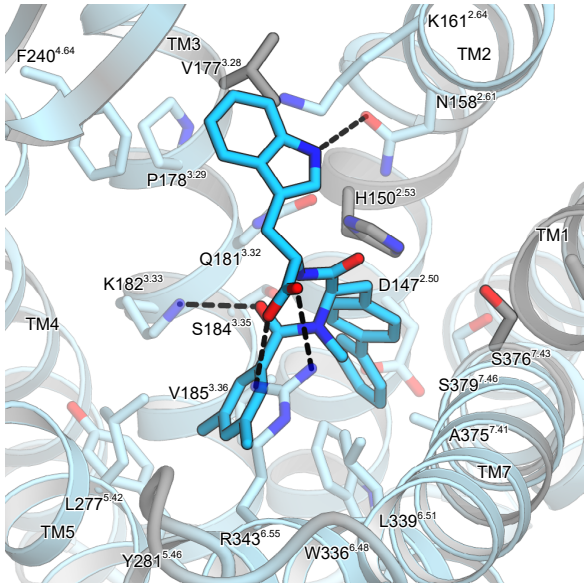

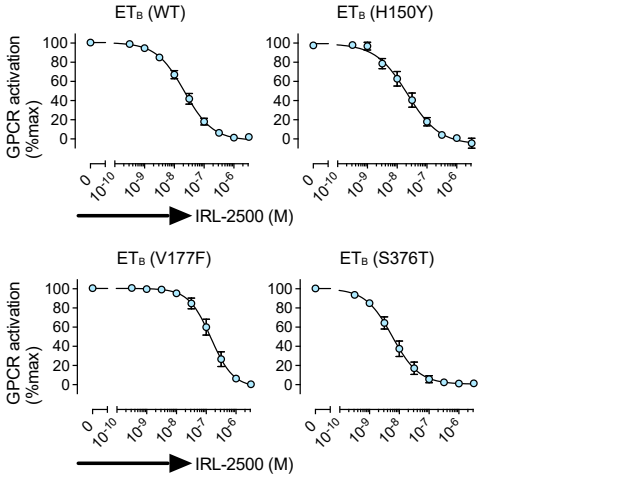

	ETB (WT)	ETB (H150Y)	ETB (V177F)	ETB (S376T)
IC_{50} (pIC_{50} ± SEM)	21 nM (7.67 ± 0.09)	18 nM (7.74 ± 0.15)	130 nM (6.87 ± 0.13)	6.1 nM (8.22 ± 0.15)

Nagiri et al. Figure 3

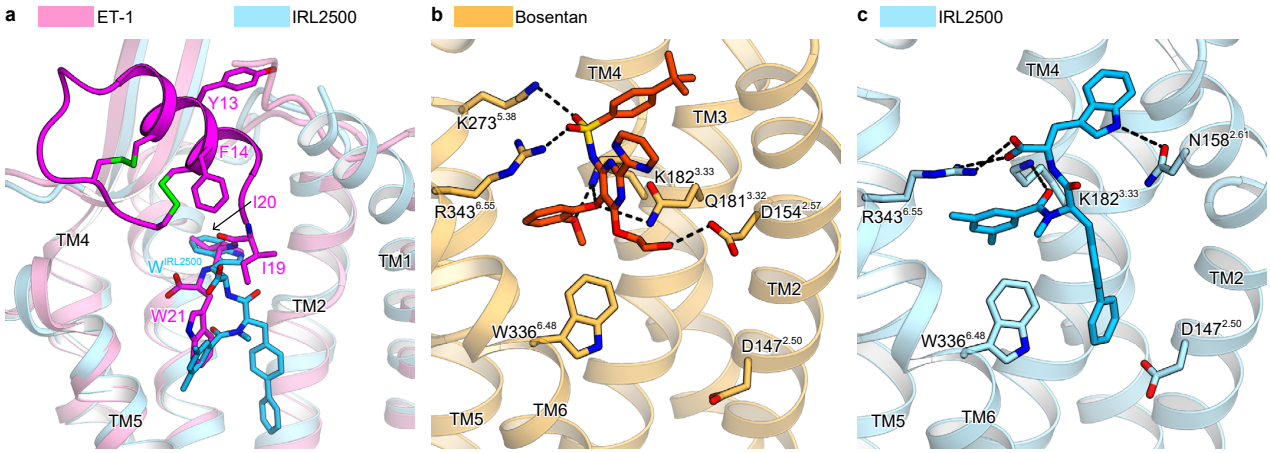

Nagiri et al. Figure 4

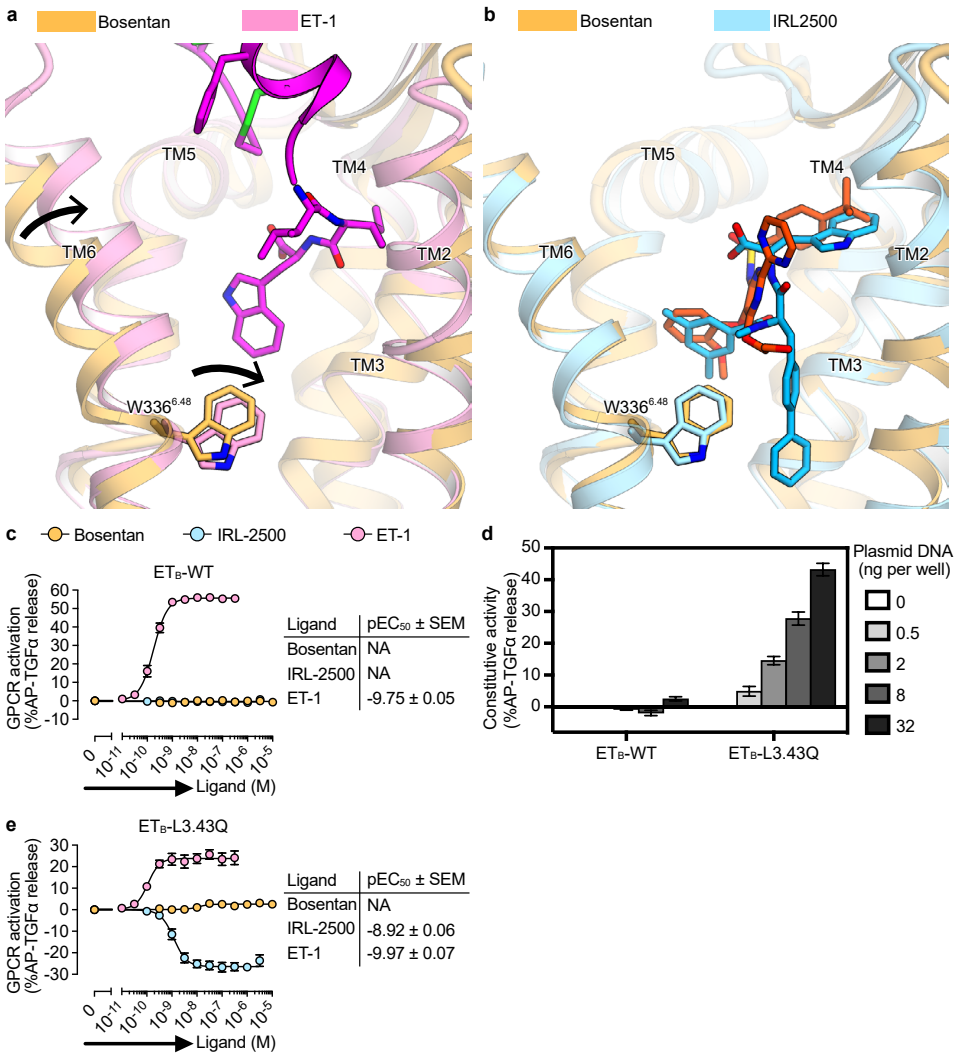

Nagiri et al. Figure 5

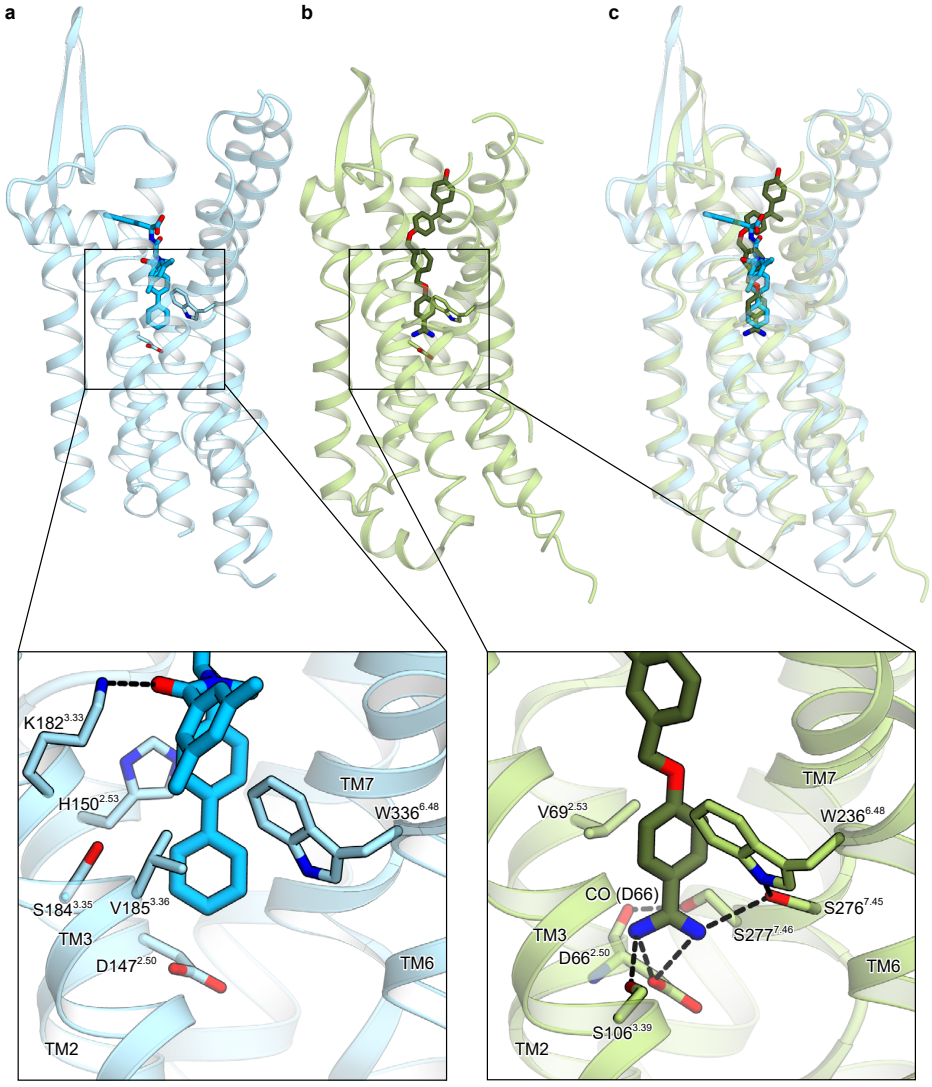

Nagiri et al. Figure 6

	IRL2500-ET_B
Data collection	
Space group	*I*422
Cell dimensions	
a, *b*, *c* (Å)	110.0, 110.0, 291.7
α, β, γ (°)	90, 90, 90
Resolution (Å)*	43.88-2.70 (2.797-2.70)
R_{meas}*	0.295 (3.946)
$\langle I/\sigma(I)\rangle$ *	10.74 (1.08)
$CC_{1/2}$*	0.995 (0.798)
Completeness (%)*	99.66 (99.35)
Redundancy*	19.3 (19.6)
Refinement	
Resolution (Å)	43.88-2.70
No. reflections	25,069
R_{work} / R_{free}	0.2244 / 0.2628
No. atoms	
Protein	3256
Ligand	43
Water/Ion/Lipid	181
Averaged *B*-factors (Å^2)	
Protein	82.9
Ligand/ion	52.3
Water	87.7
R.m.s. deviations from ideal	
Bond lengths (Å)	0.004
Bond angles (°)	0.92
Ramachandran plot	
Favored (%)	97.77
Allowed (%)	2.23
Outlier (%)	0

*Values in parentheses are for highest-resolution shell.

Nagiri et al. Table 1

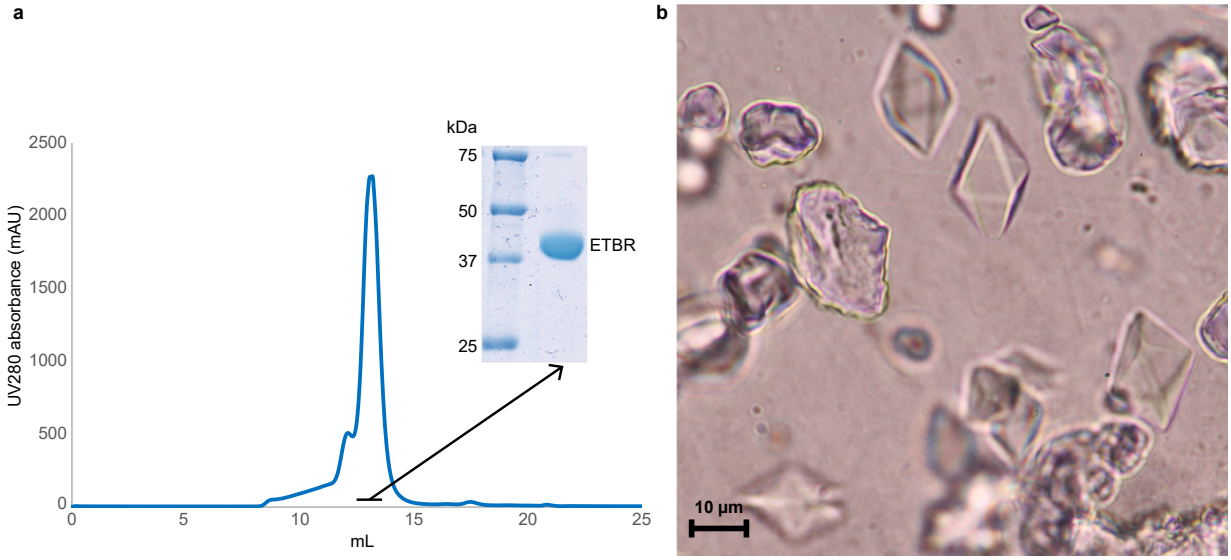

Nagiri et al. Fig. S1

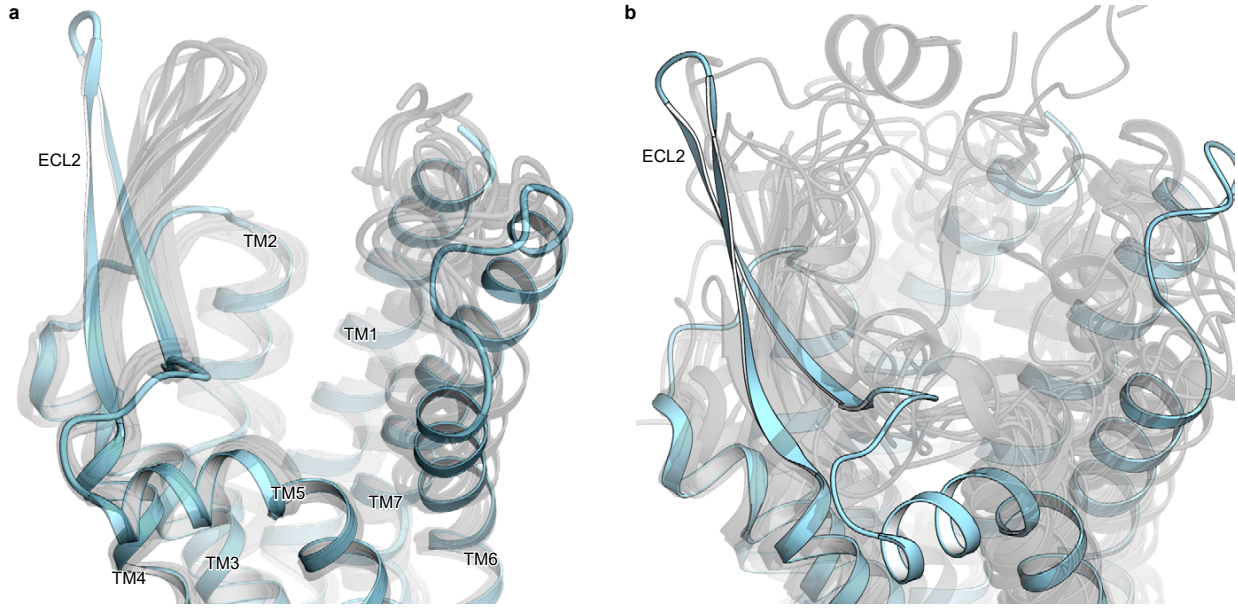

Nagiri et al. Fig. S2

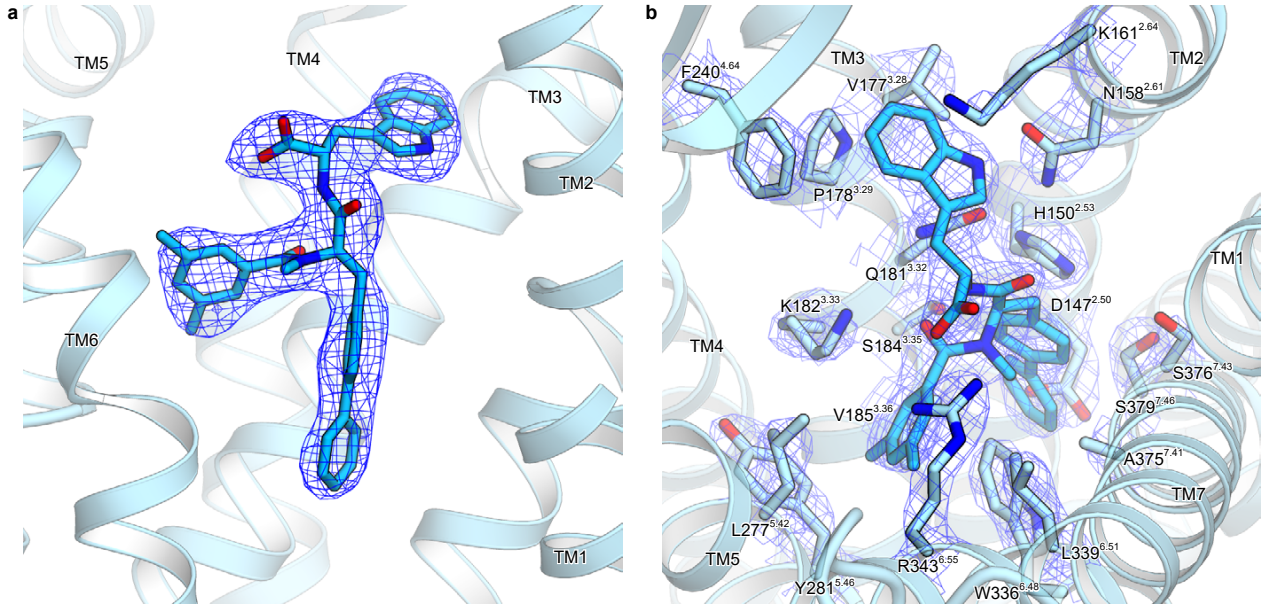

Nagiri et al. Fig. S3

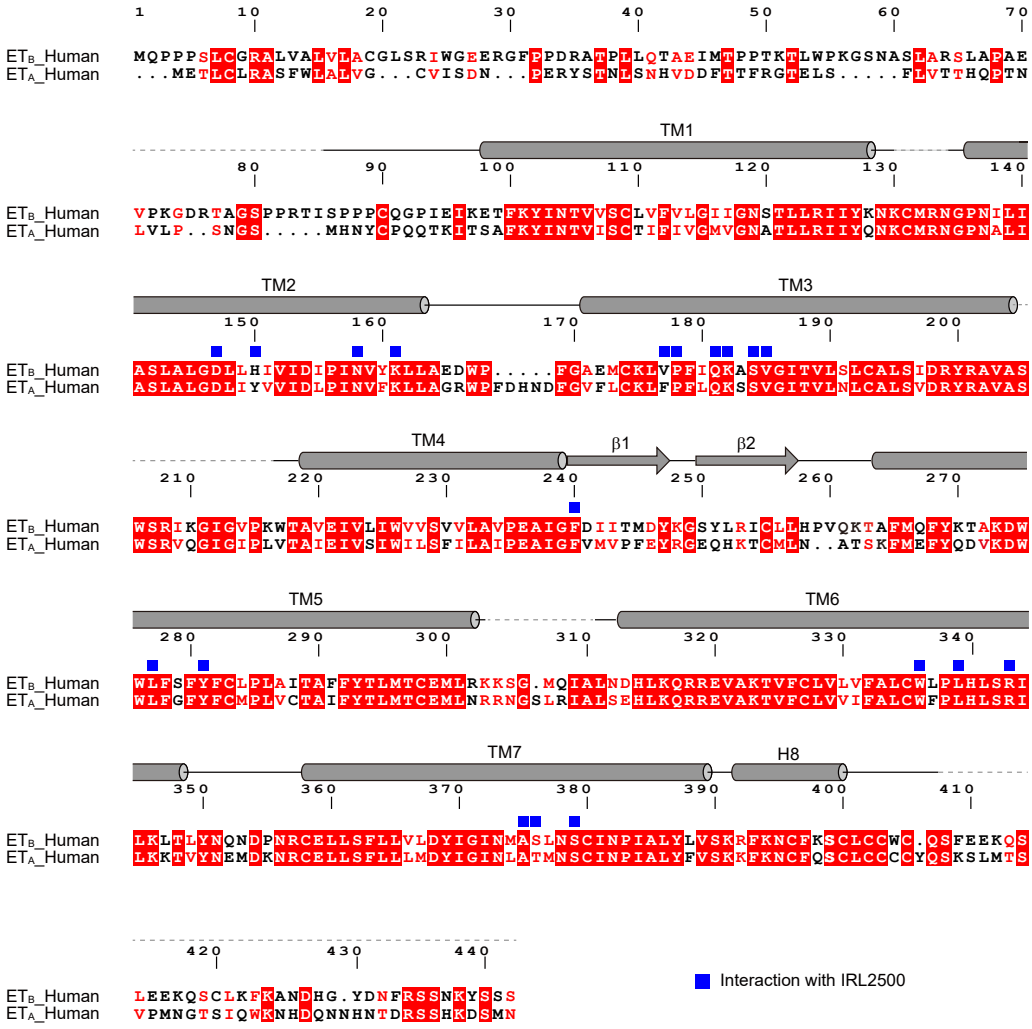

Nagiri et al. Fig. S4

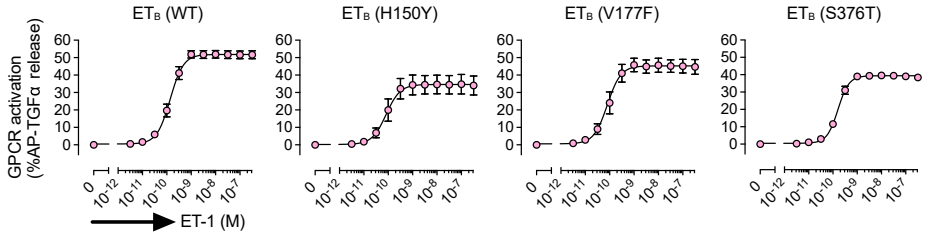

	ETB (WT)	ETB (H150Y)	ETB (V177F)	ETB (S376T)
EC50	0.14 nM	0.090 nM	0.093 nM	0.16 nM
(pEC50 ± SEM)	(9.85 ± 0.07)	(10.05 ± 0.10)	(10.03 ± 0.11)	(9.79 ± 0.04)

Nagiri et al. Fig. S5